Azole energetic materials: Initial mechanisms for the energy release from electronical excited nitropyrazoles

Bing Yuan, Zijun Yu, and Elliot R. Bernstein

Azole energetic materials: Initial mechanisms for the energy release from electronical excited nitropyrazoles

Bing Yuan, Zijun Yu, and Elliot R. Bernstein[a]
Department of Chemistry, Colorado State University, Fort Collins, Colorado 80523-1872, USA

Decomposition of energetic material 3,4-dinitropyrazole (DNP) and two model molecules 4-nitropyrazole and 1-nitropyrazole is investigated both theoretically and experimentally. The initial decomposition mechanisms for these three nitropyrazoles are explored with complete active space self-consistent field (CASSCF) level. The NO molecule is observed as an initial decomposition product from all three materials subsequent to UV excitation. Observed NO products are rotationally cold (<50 K) for all three systems. The vibrational temperature of the NO product from DNP is (3850 $\pm$ 50) K, 1350 K hotter than that of the two model species. Potential energy surface calculations at the CASSCF(12,8)/6-31+G(d) level illustrate that conical intersections plays an essential role in the decomposition mechanism. Electronically excited S_2 nitropyraozles can nonradiatively relax to lower electronic states through $(S_2/S_1)_{CI}$ and $(S_1/S_0)_{CI}$ conical intersection and undergo a nitro-nitrite isomerization to generate NO product either in the S_1 state or S_0 state. In model systems, NO is generated in the S_1 state, while in the energetic material DNP, NO is produced on the ground state surface, as the S_1 decomposition pathway is energetically unavailable. The theoretically predicted mechanism is consistent with the experimental results, as DNP decomposes in a lower electronic state than do the model systems and thus the vibrational energy in the NO product from DNP should be hotter than from the model systems. The observed rotational energy distributions for NO are consistent with the final structures of the respective transition states for each molecule. © *2014 AIP Publishing LLC*. [http://dx.doi.org/10.1063/1.4861670]

I. INTRODUCTION

Energetic materials are relatively sensitive to external perturbations: sparks, shocks, heat, or arc scan cause them to release a large amount of energy, enough to sustain detonation. An important goal of energetic material research is to find new energetic molecules with both high energy storage capacity and detonation performance, but with improved thermal stability and impact/shock resistance in order to minimize the risk of accidental discharge. Environmental and toxicity issues also play an essential role in the search for new energetic molecules.[1–9] Recently, the energetic species 3,4-dinitropyrazole (DNP) has become a focus of interest for its ability to be melt-cast: it can be a replacement for older energetic materials, such as TNT.[9]

Azoles are N-heterocyclic aromatic molecules with a five-member ring, containing only carbon and nitrogen atoms[10] (see Figure 1 for the ring numbering system). The reactivity of DNP has been studied by quantum chemical methods to determine the electrophilic and nucleophilic positions on the pyrazole ring.[11] The explosive sensitivity upon the formation of molecule-cation interactions between the nitro groups of DNP and cations in the groups 1 and 2 of the periodic table[9] along with the aqueous solubility of DNP[12] have also been studied. Nonetheless, the mechanisms and dynamics of DNP decomposition at the molecular level is

still unclear: further research into these issues is required to elucidate the energy storage properties of azoles in general and pyrazoles in particular.

As a valuable intermediate and first step for understanding such behavior for energetic DNP, several research groups have studied properties of pyrazoles with a single nitro group.[10, 13–17] Based on calculations and spectroscopic studies, the electrostatic potentials and frontier molecular orbital energies of simple mono-nitropyrazoles have been evaluated: the electron-withdrawing group NO_2 is found to lower the HOMO/LUMO energy gap and increase the reactivity of pyrazole compounds.[13] Studies of protonation constants for nitropyrazoles suggest that the effect of the nitro group on azole chemistry depends on its position on the ring: the effect is stronger if the nitro group is close to the N atom of the pyrazole ring.[13, 14] Thermal decomposition studies (25–250 °C) of nitropyrazole compounds give their stability in the order 3 → 4 → 1-nitropyrazole >pyrazole.[15] Using time-resolved pulsed photoacoustic spectroscopy to excite some of the resonant modes of compounds at different temperatures, NO_2 is observed as a major ground electronic state product and the same stability orders are found.[16] The properties of pyrazoles substituted with NO_2 at different pyrazole ring positions are quite useful for further studies of DNP. The more NO_2 groups on the pyrazole ring the less stable the molecule becomes. Nonetheless, detailed comparisons between energetic dinitro- and non-energetic (model) mono nitro-pyrazole molecules with regard to their decomposition reactions and mechanisms should prove very illuminating and

---

[a]Author to whom correspondence should be addressed. Electronic mail: erb@lamar.Colostate.edu
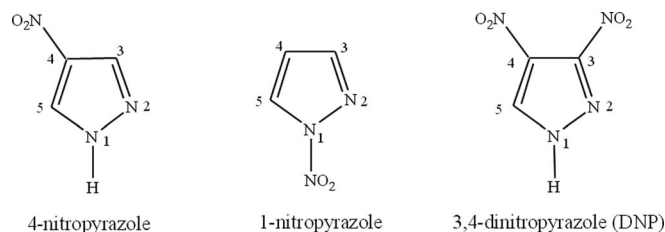
FIG. 1. Chemical structures of 4-nitropyrazole, 1-nitropyrazole, and DNP.

insightful, as at present the mechanistic differences between energetic and model system behavior is not understood for these species.

Many energetic materials are organic molecules with NO_2 groups bonded to a carbon, nitrogen, or oxygen atom. From previous studies, the initial step in the decomposition process of these isolated molecules, following electronic excitation, is $X-NO_2$ (X = C,N,O) to X-ONO isomerization (a nitro-to-nitrite, unimolecular reaction): the isomerized species then decomposes to form an NO product.[3,18] Electronic excitation of condensed phase energetic species has been suggested and recognized as a major factor in the release of stored energy from energetic molecules over the past 50 years.[1–6,18–23] In this instance, conical intersections between different potential energy surfaces play a key role in the ultrafast ($\sim$100 fs) decomposition mechanisms.[5,6,24] In nonadiabatic unimolecular chemistry, a conical intersection is the crossing (interaction) point between two electronic states or two potential energy surfaces: conical intersections are widely employed to explain and understand the excited state chemistry of organic and inorganic molecules. In our previous study of energetic and model molecules, including 1,3,5-trinitro-1,3,5-triazacclohexane (RDX), 1,3,5,7-tetranitro-1,3,5,7-tetraazacyclooctane (HXM), Hexanitrohexaazaisowurtzitane (CL-20), s-tetrazine, 3-amino-6-chloro-1,2,4,5-tetrazine-2,4-dioxide (ACTO), 3,6-diamino-1,2,4,5-tetrazine-1,4-dioxide (DATO), diaminofurazan (DAF), furazan, pentaerythritol tetranitrate (PETN), 2-nitroimidazole, 4-nitroimidazole, 1-methyl-5-nitroimidazole, and dimethylnitramine (DMNA), the existence of conical intersections in the X-ONO isomerization reaction coordinate provides a direct, nonadiabatic, decomposition pathway in the excited state, which successfully explains the experimental observations.[25–27,29–32,34–38]

In this work, we focus on understanding the first-step in the unimolecular decomposition mechanisms for the energetic material 3,4-dinitropyrazole and two model, nonenergetic molecules 1-nitropyrazole and 4-nitropyrazole, following electronic excitation. Experimentally, energy resolved spectroscopy is studied to define dynamics of the reaction through elucidating the rotational and vibrational temperatures of the initial decomposition product NO. Employing quantum chemistry calculations (Gaussian 09, CASSCF), potential energy surfaces for a number of excited states and the ground electronic state are explored. The detailed decomposition mechanisms for these three molecules are determined and discussed. Through comparisons between energetic and model molecules, a more complete comprehension of the

energetic molecule properties obtains. Such insights can be employed to develop new and better energy storage materials for both general use and specific purposes.

II. EXPERIMENTAL PROCEDURES

The experimental setup consists of a matrix-assisted laser desorption (MALD) system, a supersonic jet expansion nozzle, and a time of flight mass spectrometer. Details of the instrumental design are described in our previous papers.[25,26] The nozzle used for the molecular beam generation is constructed from a Jordan Co. pulsed valve and a laser ablation attachment. The laser desorption head is attached to the front of the pulsed valve with three significant parts: (1) a 2×60 mm channel for the expansion gas from the nozzle, (2) a conical channel (3 mm at the outside and 1 mm at the intersection with gas expansion channel) for the ablation laser beam perpendicular to the expansion gas channel, and (3) a 40 mm diameter hole for the sample drum. The sample drum fits into the 40 mm hole and is simultaneously rotated and translated by a motor and gear system in the vacuum in order to present a fresh sample region to the ablation laser for each pulse. The nonvolatile samples are desorbed from the drum by 532 nm ablation laser, entrained in the flow of He carried gas under a pressure of 80 psi through the 2×60 mm channel in the laser desorption head and expanded into the vacuum chamber. With 80 psi He backing pressure for the closed pulsed valve, the chamber pressure remains 2×10^{-7} torr; with the valve open at 10 Hz, the chamber pressure increases to 4×10^{-7} torr.

All sample drums for MALD are prepared by wrapping a piece of porous filter paper around a clean Al drum. A solution of 0.02 mol/l matrix (R6G) and 0.01 mol/l sample in acetone is uniformly sprayed on the drum surface while it is rotating under a halogen heat lamp in a fume hood to make sure the sample coating is dry. An air atomizing spray nozzle (Spraying System Co.) with siphon pressure of 10 psi is used to deposit sample plus matrix on the filter paper surface. The dried drum with well-distributed sample is then placed in the laser ablation head assembly and put into the vacuum chamber for decomposition reaction studies. The DNP is supplied by Dr. Rao Surapaneni and Mr. Reddy Damavarapu (ARL, Picatinny Arsenal, N.J.). 1-nitropyraozle and 4-nitropyrazole are bought from Sigma-aldrich Co. at 98% and 97% purity, respectively.

In addition to ablation laser, one or two others laser are required to photoexcite the sample in the beam and then detect the photo dissociated fragments. For NO detection, a single pump/probe laser is used at 226/236/248 nm to both initiation of energetic sample and detection of the NO product following a one color (1+1) resonance-enhanced two photon ionization (R2PI) scheme [A(v$'$ = 0) $\leftarrow$ X(v$''$ = 0-2) and I $\leftarrow$ A transitions] through TOFMS. The proper UV laser wavelengths for this process are generated by a dye laser, pumped by the second harmonic (532 nm) of a Nd: yttrium aluminum garnet laser's fundamental output (1.064 μm), in conjunction with a wavelength extension system. The typical pulse energy of the UV laser is 70–700 μJ/pulse, which gives an intensity of $\sim$2.0 $\times$ 10^7–2.8 $\times$ 10^8 W/cm^2 for a 8 ns pulse

duration. The spectra are not saturated and only single photon absorption occurs for the sample and the NO product at $\sim 50\ \mu$J/pulse between 248 and 226 nm. The molecular beam is perpendicularly crossed by the UV laser beam, which is focused to a spot size of about 0.2 mm diameter at the ionization region of the TOFMS.

The timing sequence of pulsed nozzle, ablation laser, and excitation/ionization laser are controlled by time delay generators (SRS DG535). The experiment is run at a repetition rate of 10 Hz. Ion signals in the TOFMS are detected by a microchannel plate (MCP) and signals are recorded and processed on a personal computer (PC) using an ADC card (Analog Devices RTI-800) and a boxcar averager (SRS SR 250).

III. COMPUTATIONAL METHODS

All calculations are executed at the CASSCF(12,8)/6-31+G(d) level of theory with the Gaussian 09 program. No symmetry restrictions are applied for the calculations. Equilibrium geometry calculations are conducted taking the total charge as neutral and the spin multiplicity as 1. To explore the excited state potential energy surfaces, the active space comprises 12 electrons distributed in 8 orbitals, denoted as CASSCF (12,8). Orbitals used for the 4-nitropyrazole active space are two π-bonding orbitals of the five-member ring π_1 and π_2, two NO nonbonding orbital $n\sigma_{NO1}$ and $n\sigma_{NO2}$, one π-nonbonding orbital $n\pi_O$, one σ nonbonding orbital $n\sigma_O$, one delocalized ONO π-antibonding orbital π_{ONO}^*, and one π-antibonding orbital of the five member ring π^* as shown in Figure 2(a). Orbitals of 1-nitropyrazole are similar. Orbitals used for the DNP active space are shown in Figure 2(b); they include two π-nonbonding orbital π_{ONO-C4} and π_{ONO-C3}, three σ nonbonding orbital $n\sigma_{NO-C3(1)}$, $n\sigma_{NO-C3(2)}$, and $n\sigma_{NO-C4}$, one π-nonbonding orbital of the five-member ring π_{RING}, and two delocalized ONO π-antibonding orbital π_{ONO-C4}^* and π_{ONO-C3}^*. To avoid convergence failure problems, a reduced (6,5) active space is also used initially for the excited state calculations: the CASSCF(12,8) is applied to get a more accurate energy values. At the larger CASSCF level orbitals for NO$_2$ and the five-member ring in DNP/single nitropyraozles are coupled and interact with each other. This interaction under the larger CASSCF is especially important for representation of highly excited states. Excitation energies are calculated by state averaging over the ground and excited states with equal weights for each state. Larger basis sets than 6-31(d) for these CASSCF calculations do not substantially improve the results and understanding of the reaction mechanisms.[37]

Critical points (minima and transition state structures) are characterized by analytical frequency calculations, and minimum energy paths are calculated using an intrinsic reaction coordinate (IRC) algorithm implemented in the Gaussian 09. DNP contains two different NO$_2$ groups which are not symmetric and to calculate the different reaction paths and critical points (conical intersections and transition states) with certain C-NO$_2$ bond breaking, CASSCF(6,5) is employed in the beginning with chosen NO$_2$ orbitals located only on one NO$_2$ group. Following this, the (12,8) active space is applied
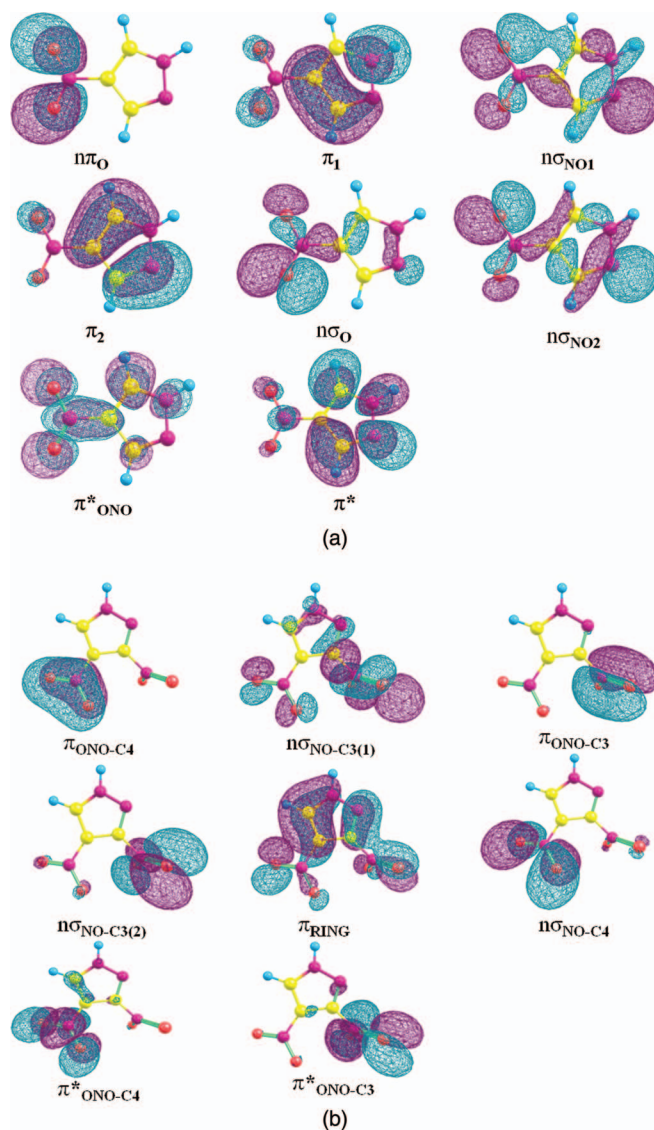

FIG. 2. (a) Orbitals used in the active space for CASSCF calculations for 4-nitropyrazole. The (12,8) active space comprises nonbonding orbitals, bonding, and antibonding π orbitals. Similar orbitals are employed to describe the states of 1-nitropyrazole. (b) Orbitals used in the active space for CASSCF calculations for 3,4-dinitropyrazole (DNP).

to get a better potential energy surface. To find the transition states and intermediate states along the reaction pathways, a relaxed scan optimization algorithm as implemented is employed in which all geometrical parameters except for the specified bond distance are optimized and electronic energies are monitored as the specified bond is elongated. In the scan, the structure with peak potential energy is most likely a transition state, and the structure with potential energy in a valley is most likely an intermediate state. To verify this conclusion and obtain a more accurate potential energy surface for the transition/intermediate states, the molecular structure provided in the scan is used as the initial structure in the following optimization calculation with CASSCF(12,8) as the active space. The accuracies of the calculations along the reaction pathway are difficult to estimate since experimental information about the conical intersections and the transition states is not available. Calculations presented in this paper,

however, are based on the experimental observations including decomposition products and the internal energy distributions within these products. Therefore, the proposed reaction pathways based on the computational results provide a reasonable and, at minimum qualitative, interpretation for the experimental observations.

IV. EXPERIMENTAL RESULTS AND DISCUSSION

NO product is observed as a major decomposition product from electronically excited DNP at 226/236/248 nm by TOFMS. The 226/236/248 nm excitation wavelength also corresponds to the resonance (0-0)/(0-1)/(0-2) vibronic bands of the $A^2\Sigma^+ \leftarrow X^2\Pi$ electronic transition of the NO product. Therefore, by scanning these laser excitation wavelengths, a (1+1) R2PI rotationally resolved spectrum of the NO product from DNP obtains. The line width of the NO mass peak is 10 ns (the laser pulse width), consistent with that expected for decomposition from the lowest few excited states. If DNP were to absorb two or more photons sequentially, the NO mass signal would broaden as we have reported earlier.[27] Thus, the NO product is associated with single photon absorption for these three samples. In this experiment, laser beam intensity is varied without change in the NO TOFMS line width, so that multiphoton dissociation of DNP is unlikely. Excited electronic states of DNP, which might be generated in the ablation process, are effectively relaxed and cooled in the highly collisional expansion process, through the supersonic nozzle.

Figure 3 shows the spectra of three different A (v' = 0) ← X(v'' = 0,1,2) rovibronic transitions of the NO molecule generated from DNP excited to its first excited electronic state. All spectra have similar rotational patterns but a varying vibrational intensity for each vibronic band. The most intense figure in each spectrum of NO corresponds to the $(Q_{11}+P_{12})$ band and the lower intensity features
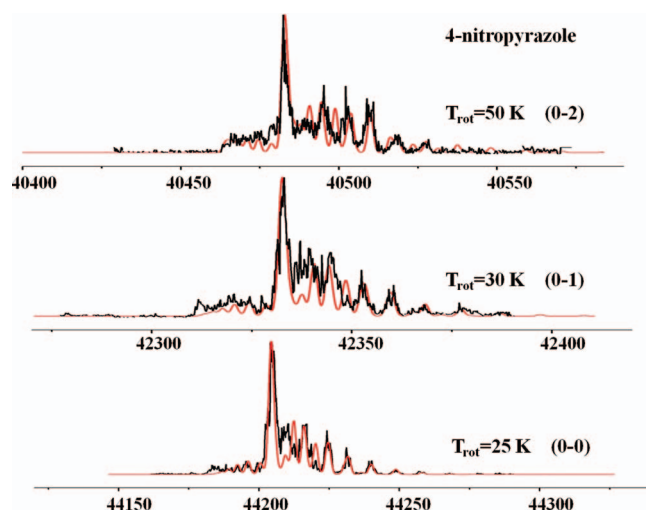

FIG. 3. One color (1+1) R2PI spectra of the vibronic transitions $A^2\Sigma^+(v' = 0) \leftarrow X^2\Pi(v'' = 0,1,2)$ of the NO product from the excited electronic state decomposition of DNP. Rotational simulations with a Boltzmann population distribution show that the three observed vibrational levels of the ground electronic state have a similar rotational temperature of ~25 K with ±10 K uncertainty. The black line is the experimental data and the red one is the theoretical simulation for NO (A-X) transition at rotational temperature 25 K.

for each vibronic transition correspond to other rotational transitions.[28] Spectral simulations based on Boltzmann population distributions for the three vibronic transitions of the NO product from DNP produce similar rotational temperatures (25 ± 10 K) for the three vibrational levels (v'' = 0,1,2) in the ground electronic state of NO. The vibrational temperature of the NO product can be obtained by simulating the relative intensities among the observed vibronic bonds, using a Boltzmann population distribution analysis and the Frank-Condon factors. The vibrational temperature of NO product from DNP is calculated to be (3850 ± 50) K and details of the vibrational temperature calculation will be described below. In summary, the NO product from electronically excited DNP has a low rotational temperature and a hot vibrational temperature, which is similar to our previous results for all NO_2 containing energetic molecules.

Even though the MALD technique is known to desorb easily fragile molecules in the gas phase without fragmentation, NO product is proven to be created in the excitation region in our previous study in three ways: comparison of NO velocity distributions from the nozzle, determination of arrival time for the NO signal intensity as a function of nozzle/pump laser timing, and NO rotational and vibrational temperature determination as a function of source of NO.[25]

NO product can be produced from several possible ways, including N-O bond breaking after nitro-nitrite isomerization, NO_2 photolysis, and HONO elimination. In our previous study of NO_2 photolysis, the rotational temperature of NO product from the expansion cooled NO_2 gas is about 130 K for the A(v' = 0) ← X(v'' = 0) vibronic transition and the temperature goes up to 400 K for vibronic transition A(v' = 0) ← X(v'' = 1). As the rotational temperature of the NO product from DNP is much lower than that for NO_2 photolysis, NO_2 is not the precursor for NO product, and NO_2 loss is not the major reaction channel for the decomposition of electronically excited DNP. The observed rotational and vibrational temperatures assigned for NO in these experiments show clearly that the NO must come from decomposition of nitropyrazoles and not NO_2.[25,29–31] HONO is also one of the possible intermediates in the formation of NO from DNP or single nitro-pyrazoles. HONO elimination for previously studied X-NO_2 system is less than 5% of the total NO elimination following the nitro-nitrite isomerization; moreover, the rotational temperature of NO product from HONO photolysis is extremely high.[25,29] Based on calculations for 4-nitropyrazole, the energy required for HONO elimination on the ground state surface is 107 kcal/mol, 21 kcal/mol higher than for the formation of NO through the nitro-nitrite isomerization, which makes HONO elimination less likely in nitropyrazoles: this result is similar to those for the nitro-imidazole sysems.[32] Thus, neither the NO_2 loss channel nor the HONO channel is present as a competitor to the nitro-nitrite isomerization/NO elimination channel.

In efforts to improve our understanding of the excited state decomposition mechanisms of DNP, two model molecules 1-nitropyrazole and 4-nitropyrazole are explored. Figure 4 and Figure 1S in the supplementary material[39] illustrate the A ← X (0-0,1,2) transition spectra with rotational spectra simulations for the initial decomposition product NO
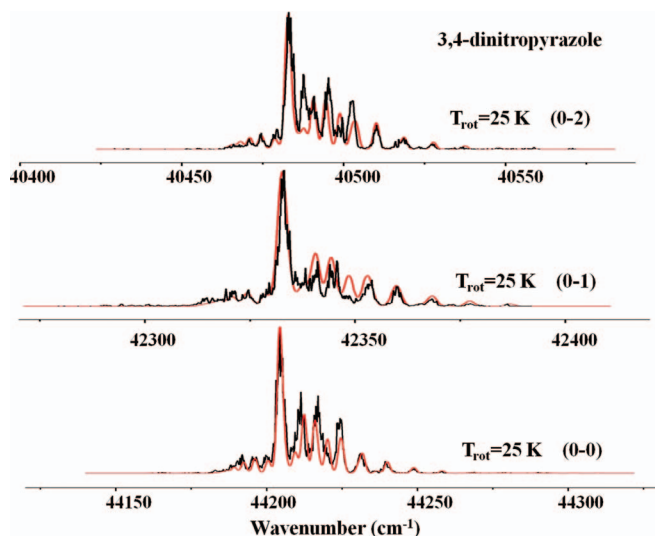
FIG. 4. One color (1 + 1) R2PI spectra of the vibronic transitions $A^2\Sigma^+(v' = 0) \leftarrow X^2\Pi(v'' = 0,1,2)$ of the NO product from the excited electronic state decomposition of 4-nitropyrazole. Rotational simulations with a Boltzmann population distribution show that the rotation temperatures of the three observed vibrational levels on the ground electronic state (0-0), (0-1), and (0-2) are 25 K, 30 K, and 50 K, respectively, with ±10 K uncertainty. The black line is the experimental data and the red one is theoretical simulation for NO (A-X) transition at rotational temperature 25 K, 30 K, and 50 K from (0-0) to (0-2).

for the two model molecules. The simulated rotational temperatures for these two model molecules are similar and both increase from (25 ± 10) K to (50 ± 10) K as the vibronic bands change from the (0-0) to (0-2) transition. The vibrational temperatures of NO from the two model materials are both calculated to be (2300 ± 300) K, 1350 K lower than NO from the energetic molecule DNP. The two mono nitro-pyrazoles may follow similar decomposition routes, but they should be different from that followed by the energetic material DNP.

The rotational and vibrational temperatures for the NO product from the three materials in the experiment are summarized in Table I. The signal intensities for the NO product of 4-nitropyrazole, 1-nitropyrazole, and DNP at different vibrational transitions A(v' = 0) ← X(v'' = 0,1,2) and transition ratios I(0-2)/(0-0) and I(0-1)/(0-0) are summarized in Table II and the Franck-Condon factors for the NO (A-X) transition in the temperature range from 1900 K to 4000 K are listed in Table III. The Franck-Condon factors are calculated using the program, Lifbase: Data Base and Spectra Simulation (version 2.1.1). For the rotational temperature range 25–50 K, these simulated Franck-Condon factors are

TABLE I. Rotational and vibrational temperatures for NO product from DNP, 1-nitropyrazole, and 4-nitropyrazole. The uncertainty of experimental rotational temperature is ±10 K.

	NO rotational temperature (K)			Vibrational
	0-0	0-1	0-2	temperature (K)
3,4-dinitropyrazole (DNP, energetic)	25	25	25	3850 ± 50
4-nitropyrazole	25	30	50	2300 ± 300
1-nitropyrazole	25	35	50	2300 ± 300

unchanged. For NO from 4-nitropyrazole, the experimental I(0-1)/(0-0) ratio equals 0.36, yielding a vibrational temperature of about 2600 K from Table III. The I(0-2)/(0-0) ratio for NO from 4-nitropyrazole is 0.068 which gives a ~2000 K vibrational temperature in Table III. The two values are different due to experimental uncertainties; for example, laser intensity is not stable, sample spaying is not exactly uniform, etc. The vibrational temperature of 4-nitropyrazole is determined to be (2300 ± 300) K. Similarly, the vibrational temperature of NO from 1-nitropyraozle and 3,4-dinitropyraozle are (2300 ± 300) K and (3850 ± 50) K, respectively.

The experimental results prove that NO is a primary decomposition product of DNP and the NO product from DNP has a low rotational temperature and a high vibrational temperature. The reaction decomposition mechanisms of energetic material DNP and model molecules should be different as the vibrational temperature of the NO product from DNP is 1350 K higher than that of NO from the model molecules. The NO product from DNP is most likely formed in a lower electronic state than that of the model molecules: the details of the reaction mechanism and reaction potential energy surfaces will be discussed based on the theoretical calculations presented in Sec. V.

V. THEORETICAL RESULTS AND DISCUSSION

The experimental results yield that the NO molecule is an initial nanosecond UV decomposition product for both electronically excited energetic and model systems. In order to understand the experimental data more completely, theoretical calculations of molecular geometries and energies for the Franck Condon structure, conical intersections, transition states, intermediate states, and nitro-nitrite isomerizations along the ground and excited state potential energy surfaces, are performed for the energetic system DNP and model

TABLE II. Experimental maximum signal intensities of the vibrational transitions A(v' = 0) ← X(v'' = 0,1,2) of NO product for materials 4-nitropyrazole, 1-nitropyrazole, and DNP when the laser intensity is 0.65 mJ.

	Signal intensity/V (laser intensity 0.65 mJ)			Ratios	
Materials	v = (0-0)	v = (0-1)	v = (0-2)	(0-1)/(0-0)	(0-2)/(0-0)
4-nitropyrazole	2.5	0.8	0.17	0.35	0.068
1-nitropyrazole	1.1	0.39	0.08	0.35	0.073
3,4-dinitropyrazole	4.0	1.97	1.0	0.49	0.25

TABLE III. The Frank-Condon factors for transitions (0-2)/(0-0) and (0-1)/(0-0) calculated using Lifbase: Data base and spectra simulation (version 2.1.1). I(...) is intensity for the transition ratio indicated.

Vibrational temperature/1000 K	1.9	2.0	2.1	2.5	2.6	2.7	3.8	3.9	4.0
I(0-1)/(0-0)	0.24	0.26	0.28	0.34	0.35	0.37	0.49	0.50	0.51
I(0-2)/(0-0)	0.06	0.07	0.08	0.12	0.13	0.14	0.24	0.25	0.26

systems 4-nitropyrazole and 1-nitropyrazole. The theoretical reaction paths with potential energies and molecular geometries are shown in Figures 5–8 and 2S–5S (supplementary material).[39]

Two possible decomposition mechanisms are explored in the theoretical study. The first mechanism includes an excited state decomposition through transition states and nitro-nitrite isomerization on the first excited electronic state S_1 potential energy surface. The second mechanism is a ground state decomposition process which goes through a conical intersection $(S_1/S_0)_{CI}$ between the S_1 and S_0 states followed by an S_0 nitro-nitrite isomerization. These two channels are chosen for comparison because the decomposition of energetic material DNP generates NO product with higher vibrational temperature than the model systems. The actual reaction pathway will depend on different factors, for example, the rate of internal vibrational energy redistribution, the heights of reaction barriers, and the rate of nonadiabatic transition through

FIG. 6. The structures of all the critical points and conical intersections mentioned in Figure 5 along the 4-nitropyrazole dissociation reaction path. Arrows in the structures of the transition states show the reaction coordinate associated with the imaginary frequency (I.F.).

the different conical intersections which can only be assessed by dynamical calculations.

Calculations at the CASSCF(12,8)/6-31+G(d) theoretical level are employed to determine the vertical excitation energies for 4-nitropyrazole, 1-nitropyrazole, and DNP from the ground electronic state S_0 to the first excited state S_1 and the second excited state S_2. The vertical excitation energies of the
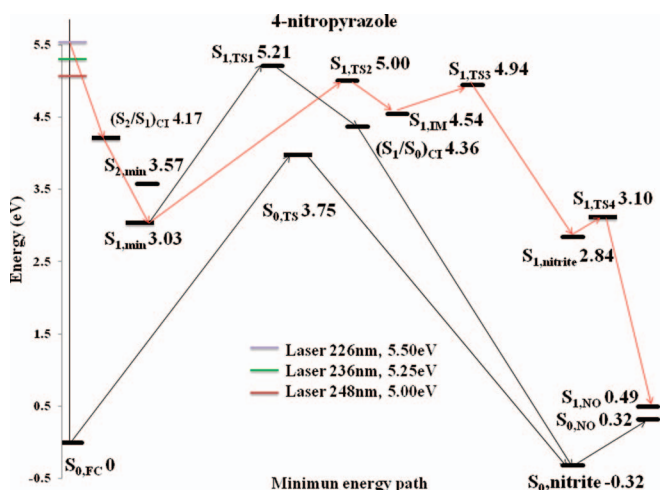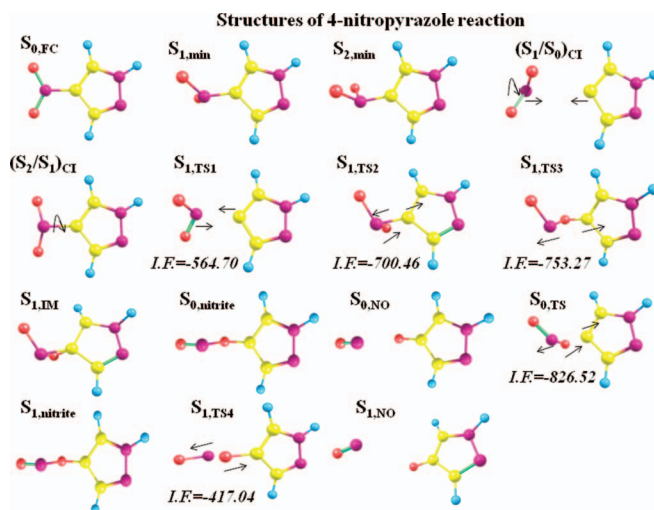

FIG. 5. A schematic one-dimensional projection of the multi-dimensional energy surfaces for 4-nitropyrazole dissociation computed at the CASSCF(12,8)/6-31+G(d) level of theory. The red arrows represent the more favorable reaction path for NO dissociation, which occurs on the excited electronic state S_1. The black arrows represent the other, less favorable, reaction path, along which NO is formed on the ground electronic state S_0. FC geometry $S_{0,FC}$ is the optimized minimum energy structure of 4-nitropyrazole on S_0. $S_{1,min}$ and $S_{2,min}$ are the structure on the first and second excited electronic states with minimum potential energy, respectively. $(S_1/S_0)_{CI}$ is the conical intersection between S_0 and S_1 states, and $(S_2/S_1)_{CI}$ is the conical intersection between S_2 and S_1 states. $S_{1,TS1}$ to $S_{1,TS4}$ are the excited transition states on the S_1 surface, $S_{0,TS}$ is transition state on the S_0 surface, and $S_{1,IM}$ is the intermediate state on S_1 state. $S_{0,nitrite}$ and $S_{1,nitrite}$ are the nitro-nitrite isomerization intermediates on the S_0 and S_1 states, respectively, and $S_{0,NO}$ and $S_{1,NO}$ are NO dissociated products on these two states.
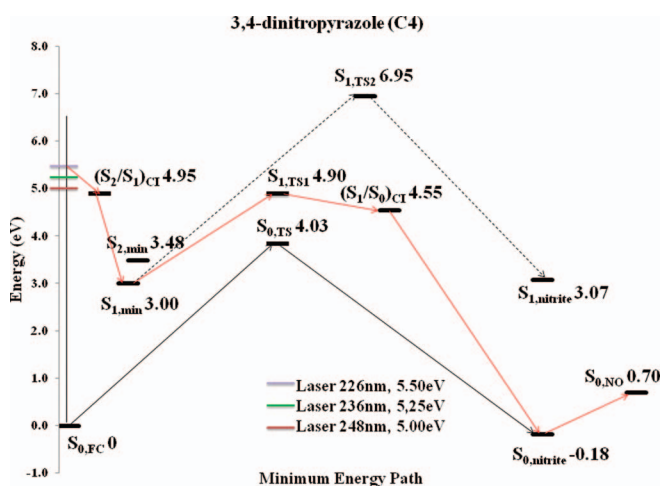

FIG. 7. A schematic one-dimensional projection of the multi-dimensional energy surfaces for 3,4-dinitropyrazole with the NO$_2$ bonded to C4 on the pyrazole ring dissociated as the first step computed at the CASSCF(12,8)/6-31+G(d) level of theory. The dashed arrows represent the reaction path of NO dissociation occurring on the excited electronic state S_1: this pathway is not available based on energy considerations. The red arrows represent the reaction path on which NO is formed on the ground electronic state S_0: this pathway is energetically allowed. FC geometry $S_{0,FC}$ is the optimized minimum energy structure of 3,4-dinitropyrazole on the ground electronic state S_0. $S_{1,min}$ and $S_{2,min}$ are the structure on the first and second excited electronic states with minimum potential energy, respectively. $(S_1/S_0)_{CI}$ is the conical intersection between S_0 and S_1 states and $(S_2/S_1)_{CI}$ is the conical intersection between S_2 and S_1 states. $S_{1,TS1}$ and $S_{1,TS2}$ are the excited transition states on the S_1 surface and $S_{0,TS}$ is transition state on the S_0 surface. $S_{0,nitrite}$ and $S_{1,nitrite}$ are the nitro-nitrite isomerization in S_0 and S_1 states, respectively, while $S_{0,NO}$ NO dissociated products in ground electronic state.
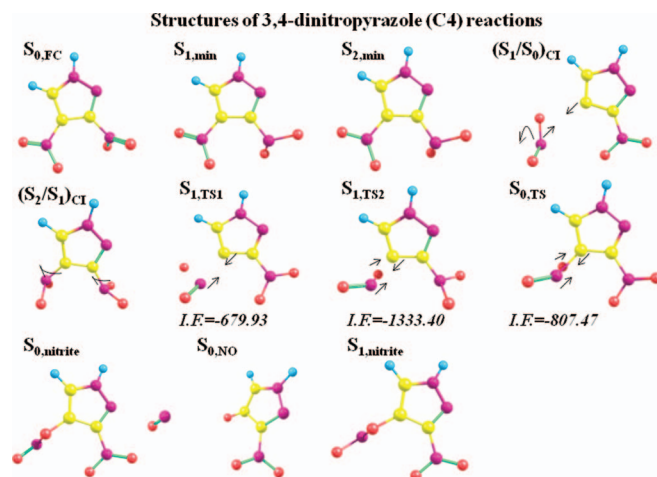
FIG. 8. The structures of all critical points and conical intersections mentioned in Figure 7 in which 3,4-dinitropyrazole with one NO_2 connected to C4 on the pyrazole ring dissociates as the first step. Arrows on the structures of the transition states show the reaction coordinates of the imaginary frequency (I.F.).

three materials are very close to the energy of single photon excitations in the range from 226 nm to 248 nm (5.0 eV to 5.5 eV) which have been used to excite these molecules. Since there is no experimental data for vertical excitation energies of nitropyrazole molecules published so far, the experimental UV-Vis absorption spectra of nitropyrazoles are taken to determine the accuracy of the CASSCF calculations. Vertical energies for the three materials and the related UV-Vis maximum absorption wavelength[14,33,34] are summarized in Table IV. As shown in Table IV, the vertical excitations calculated through CASSCF(12,8)/6-31+G(d) for the two lowest lying excited electronic states (S_1 and S_2) of 4-nitropyrazole are 4.16 eV and 4.78 eV, respectively. The UV-VIS absorption of 4-nitropyrazole has two maximum at 3.91 ± 0.67 eV and 4.62 ± 0.62 eV. This comparison reveals that the CASSCF(12,8) method gives a reasonable treatment of the relevant excited states as it falls into the commonly acceptable uncertainty range of ± 0.5 eV. Similarly, CASSCF(12,8) calculation for 1-nitropyrazole and DNP are also reasonable as the theoretical value is close to the experimental data. The CASSCF calculations show that the two lowest-lying excited states (S_1 and S_2) for two model materials are (n,π^*) transitions from the σ nonbonding orbital $n\sigma_O$ (S_1) or $n\sigma_{NO}$ (S_2) of NO_2 to delocalized ONO π-antibonding orbital π^*_{ONO}. In the third electronic state S_3, the transition becomes (π,π^*)

from π-bonding orbitals of the five-member ring π_1 or π_2 to π^*_{ONO} (orbitals shown in Figure 2(a)). The three lowest-lying excited states (S_1 to S_3) for DNP are (n,π^*) transitions from the σ nonbonding orbital $n\sigma_{NO}$ of NO_2 to delocalized ONO π-antibonding orbital π^*_{ONO} of NO_2. The transition to the S_1 state is from $n\sigma_{NO\text{-}C3(1)}$ of NO_2 on C3 to $\pi^*_{NON\text{-}C3}$ of NO_2 on C3, to the S_2 state is from $n\sigma_{NO\text{-}C4}$ on C4 to $\pi^*_{NON\text{-}C4}$ on C4, and to the S_3 state is from the other σ nonbonding orbital $n\sigma_{NO\text{-}C3(2)}$ on C3 to $\pi^*_{NON\text{-}C3}$ on C3 (orbitals shown in Figure 2(b)). From CIS calculations, the four lowest transition of DNP are all (n,π^*) and the fifth one becomes (π,π^*) as DNP contains one more NO_2 group than model systems. These transitions are similar to those found for the nitro-imidazole systems in previous study.[31,32] The potential energy surfaces for the S_3 state of these three molecules are above the laser excitation maximum. Thus, the S_3 state is not considered in the potential energy surface calculations. From our previous studies, enlarging the basis set does not significantly improve the relative excitation energies of critical points, and therefore, a 6-31+G(d) basis set is used for all calculations to maintain optimum conditions for computational cost, accuracy, and comparisons.

A. Calculations for 4-nitropyrazole

A schematic one-dimensional projection of the multidimensional singlet potential energy surfaces (S_0, S_1 and S_2) of 4-nitropyrazole with locations and potential energies (the presented energies are not corrected for zero point energy) for different critical points and conical intersections along the minimum energy reaction path is plotted in Figure 5. The reaction coordinates depicted in Figure 5 include C-N bond lengths, ONC bond angles, and ONCC dihedral angles of the active site of 4-nitropyrazole. Arrows in Figure 5 indicate different possible channels for 4-nitropyrazole decomposition. The structures of each critical point and conical intersection are summarized in Figure 6 and arrows near the transition states and conical intersections show the imaginary frequencies (I.F.). In Figures 5 and 6, FC geometry $S_{0,FC}$ is the optimized minimum energy, planar structure of 4-nitropyrazole on the S_0 state. $(S_1/S_0)_{CI}$ is the conical intersection between the S_0 and S_1 states and $(S_2/S_1)_{CI}$ is the conical intersection between the S_2 and S_1 states. $S_{1,TS1}$ to $S_{1,TS4}$ are the excited transition states on the S_1 surface and $S_{1,IM}$ is the intermediate state. $S_{0,nitrite}$ and $S_{1,nitrite}$ are the nitro-nitrite isomerization states on the S_0 and S_1 states, respectively, while $S_{0,NO}$ and

TABLE IV. Comparison of previous experimental data and present CASSCF calculations of vertical excitation energy S_1 and S_2 for 4-nitropyrazole, 1-nitropyrazole, and 3,4-dinitropyraozle (DNP).

	CASSCF calculation (eV)		UV-vis absorption in experiment (eV)	
	S1	S2	$\lambda_{max,1}$	$\lambda_{max,2}$
3,4-dinitropyrazole	4.20	4.78	3.97[a]	. . .
4-nitropyrazole	4.16	4.78	3.91 ± 0.67[b]	4.61 ± 0.62[b]
1-nitropyrazole	4.17	4.97	. . .	4.64[c]

[a]UV-vis absorption in 0.05 N NaOH.[34]
[b]UV-vis absorption in EtOH.[33]
[c]UV-vis absorption in 1M H_2SO_4.[14]

$S_{1,NO}$ are NO dissociated products in these two states. The optimized x, y, z coordinates in angstroms of all the stationary points for the 4-nitrpyrazole reaction are shown in Table IS(a) in the supplementary material.[39] Figure 5 shows that following excitation to the second excited electronic state S_2, 4-nitropyrazole undergoes a rapid internal conversion from the S_2 state to the S_1 state through the $(S_2/S_1)_{CI}$ conical intersection: molecules undergoing this process would store sufficient vibrational energy in the S_1 state, transferred from the S_2 electronic energy, to dissociate. In this nonadiabatic radiationless internal conversion, no significant change occurs in the nuclear configuration of 4-nitropyrazole (only some rotation of the NO_2 group) and no barrier exists. The adiabatic energy gap between the S_1 and S_2 surfaces near $(S_1/S_2)_{CI}$ is computed to be 88 cm^{-1} which means the S_1 and S_2 surfaces are strongly nonadiabatically coupled with one another and the small energy gap increases the probability of nonadiabatic transition from upper to lower electronic states. As molecules move from S_2 to S_1 through $(S_2/S_1)_{CI}$, the most favorable path for 4-nitropyrazole decomposition shown in Figure 5 is the one colored in red. Along this nitro-nitrite isomerization path, molecules surmount the energy barriers for two concerted transition states $S_{1,TS2}$ and $S_{1,TS3}$ at energies 5.00 eV and 4.94 eV. Then, 4-nitropyrazole undergoes a nitro-nitrite isomerization in the S_1 state ($S_{1,nitrite}$) and finally NO departs the pyrazole ring moiety after passing over a small barrier of 0.26 eV with respect to $S_{1,nitrite}$. $S_{1,TS2}$ and $S_{1,TS3}$ are tight transition states, the negative frequency or unstable normal mode of which is characterized by out of plane bending of the ONCC moiety (a nitro-nitrite isomerization). The IRC algorithm is associated with the bending mode of the C-NO$_2$ moiety, which ensures that these two transition states lead to the nitro-nitrite isomerization. As NO moves away from the pyrazole ring, no obvious torque is generated on the NO product. Therefore, the NO product should have a cold rotational temperature, as is consistent with the experimental results. The other possible conversion path shown in Figure 5 is that instead of decomposing on the S_1 state, 4-nitropyrazole surmounts the energy barrier of $S_{1,TS1}$(5.21 eV), undergoes another nonadiabatic internal conversion to the S_0 state through $(S_1/S_0)_{CI}$ (the energy difference between S_1 and S_0 state is 7 cm^{-1}) and decomposes on the S_0 state via $S_{0,nitrite}$ isomerization. This pathway is energy acceptable under 226 nm and 236 nm excitation, as the highest potential energy peak $S_{1,TS1}$ has lower energy than the laser source; nonetheless, this potential peak is 0.21 eV higher than the one $(S_{1,TS2})$ on the S_1 decomposition path, making the S_0 decomposition pathway less favorable. Under 248 nm excitation, the S_0 decomposition pathway for 4-nitropyrazole becomes forbidden due to energy constraints for the $S_{1,TS1}$ barrier. In sum, under 226 nm and 236 nm excitation, the decomposition of 4-nitropyrazole can occur either on the S_1 or S_0 state surfaces: the S_1 state decomposition is more favorable, however, due to a lower energy barrier. At 248 nm excitation, the decomposition can only take place on the S_1 state surface.

From the experimental results, NO product from 4-nitropyrazole has a cold rotational temperature (<50 K), which increases from (25 $\pm$ 10) K to (50 $\pm$ 10) K as the excitation energy decreases from 5.5 to 5.0 eV (226 to

248 nm). Based on the theoretical calculations, whether the molecule dissociates in the S_0 or S_1 state potential energy surfaces, no torque on the NO product is apparent, and therefore the rotational temperature of NO is low. Changing the excitation energy from 5.5 to 5.0 eV, the probability that 4-nitropyrazole decomposes on the S_0 state becomes smaller and smaller: this may explain why the experimental rotational temperature increases 25 K. Though most of the 4-nitropyrazole molecules decompose in the S_1 state, the vibrational temperature of NO product is hot (2300 $\pm$ 300 K). In the NO dissociation calculation, the molecular energy decreases quickly from $S_{1,TS4}$ (Figure 6) until the NO group is 3.5 A away from the pyrazole ring and then the energy drops 2.61 eV in this process. Following NO group dissociation, calculations for the pyrazole ring with a single oxygen attached to C4, the energy difference between S_1 and S_0 is only 0.75 eV, much smaller than the energy difference between $S_{1,nitrite}$ and $S_{0,nitrite}$ which is 3.16 eV. Thus one can concluded that during the molecular dissociation process in the S_1 state, most of the energy stored in the molecule is transferred (along the reaction coordinate) to the vibrational and translational energy of the NO product, consistent with the NO product having a relatively high vibrational temperature. Compared to the bond length 1.32 A of the NO at the nitro-nitrite isomerization, the equilibrium bond length of the NO product is 1.15 A, so that excitation of the NO vibration is reasonable.

The 4-nitropyrazole theoretical results also support that the decomposition dynamics are purely nonadiabatic in nature and that conical intersections can lead rapidly and efficiently to internal conversion from upper to lower electronic state through radiationless transition. During the internal conversion, electronic energy in the upper state is converted to vibrational energy in the lower state with a potential time scale of a few tens femtoseconds. The calculations also implicitly support the notion that though conical intersections between higher and lower energy electronic states, different parts of the lower potential energy surfaces are explored, away from the Franck-Condon equilibrium position, such that different and often unexpected chemistry can readily occur. Conical intersections are now firmly established to be the key features in the excited electronic state chemistry of polyatomic molecules.

B. Theoretical calculations for 1-nitropyrazole

A schematic one-dimensional projection of the multidimensional singlet potential energy surfaces (S_0, S_1, and S_2) of 1-nitropyrazole with locations and potential energies (the presented energies are not corrected for zero point energy) for different critical points and conical intersections along the minimum energy reaction path is plotted in Figure 2S in the supplementary material.[39] Arrows in Figure 2S indicate different possible decomposition channels for 1-nitropyrazole. Structures for each critical point and conical intersection are summarized in Figure 3S:[39] arrows near the transition states and conical intersections show the imaginary frequencies. The optimized x, y, z coordinates in angstroms of all the stationary points for the 1-nitrpyrazole reaction are shown in Table IS(b) in the supplementary material.[39] As depicted in

Figure 2S, 1-nitropyrazole is excited to its second excited electronic state S_2 (226–248 nm) and then undergoes a rapid internal conversion from S_2 to S_1 through the $(S_2/S_1)_{CI}$ conical intersection. In this nonadiabatic, radiationless internal conversion, no significant change occurs in the nuclear configuration and no barrier exists. The adiabatic energy gap between the S_1 and S_2 surfaces near $(S_1/S_2)_{CI}$ is computed to be 153 cm^{-1}. After molecules transition from the S_2 to the S_1 state through $(S_2/S_1)_{CI}$, two decomposition pathways are possible, as shown in Figure 2S. On one path, molecules surmount the energy barriers for two concerted nitro-nitrite isomerization transition states $S_{1,TS2}$ and $S_{1,TS3}$ with 3.93 eV and 3.78 eV energy on the S_1 state surface, respectively. Then the 1-nitropyrazole molecule undergoes a nitro-nitrite isomerization ($S_{1,nitrite}$), and finally NO leaves after passing a small barrier of 0.30 eV with respect to $S_{1,nitrite}$ on the S_1 state potential energy surface. $S_{1,TS2}$ and $S_{1,TS3}$ are loose transition states, the imaginary frequency is characterized by the out of plane bending of the ONCC moiety, which corresponds to a true nitro-nitrite isomerization. As NO moves away from the pyrazole ring, no obvious torque is found in the calculation acting on the NO product: the NO product should, thereby, have a cold rotational temperature. The other possible reaction path involves as follows: 1-nitropyrazole surmounts the energy barrier $S_{1,TS1}$ (3.93 eV), undergoes another nonadiabatic internal conversion through $(S_1/S_0)_{CI}$ conical intersection (the energy difference between S_1 and S_0 state is 35 cm^{-1}), and decomposition the S_0 state via the $S_{0,nitrite}$ isomerization with a small barrier of 0.42 eV. Both pathways are roughly equally probable, based on their energy values and conical intersection adiabatic separations. If the molecule goes through $(S_1/S_0)_{CI}$, it has another two possibilities on the S_0 surface: it can return to $S_{0,FC}$ (no reaction) or move to the nitro-nitrite isomerization $S_{0,nitrite}$, and finally form the NO product. Both of these two pathways are energetically acceptable and the potential energy of the molecule changes smoothly along the S_0 potential surface without any barriers. In a simple ($-\Delta E/\Delta r$) reaction force calculation, in which E is the potential energy and r is the distance along the reaction coordinate the absolute force for the $S_{0,nitrite}$ reaction coordinate is higher by a factor of three for nitro-nitrite isomerization reaction coordinate. This force difference suggests that the $S_{0,nitrite}$ pathway is more favorable as it presents a steeper descent potential energy surface. In this case, the probability of an NO product forming on the S_0 state is much greater than an NO_2 product. Thus 1-nitropyrazole is expected, based on these calculations, to generate NO as an initial decomposition product. In sum, under all three excitation conditions, the decomposition of 1-nitropyrazole can occur either on the S_1 or S_0 state potential energy surface (or perhaps both), as both reaction paths are energetically accessible and most probable for NO generation.

In the NO dissociation process, the molecular energy decreases quickly from $S_{1,TS4}$ in Figure 2S until the NO group is 3.5 A away from the pyrazole ring at which point the energy reaches a minimum: the total electronic energy decrease in this process is 2.11 eV. During the molecular decomposition on the S_1 state, most of the energy stored in the molecule is transferred to the vibrational and translational energy of the NO product. This energy transfer to the nuclear coordinates enables the NO product to have a relatively high vibrational temperature. The NO bond length at the nitro-nitrite isomerization (1.31 A), compared to the equilibrium bond length of the NO product (1.14 A), ensures significant excitation of the vibration of NO as the final O-N bond breaks.

1-nitropyrazole and 4-nitropyrazole have different NO_2 group positions on the pyrazole ring. Though the reaction mechanism is slightly different, both of them can decompose either on the S_1 electronic state or S_0 electronic state producing NO with similar cold rotational temperature and warm vibrational temperature. Compared to other model molecules, the behavior of nitropyrazole model materials is closer to the behavior of nitroimidazole based materials: unlike other model systems with hot rotational temperature for NO product, both species have relatively cold rotational temperatures (<60 K) under the same excitation conditions.[31,32] This might arise as both nitropyraozle and nitroimidazole molecules have low lying excited states (n $\rightarrow \pi^*$, S_2) transitions of the aromatic rings.

C. Theoretical calculations for 3,4-dinitropyrazole

DNP has two NO_2 groups bonded to C3 and C4 on the pyrazole ring and the decomposition of these two NO_2 group are calculated separately as the geometry of DNP is not symmetric. Conical intersections and critical points in DNP decomposition pathways are explored by considering only one NO_2 group as the active site located at a particular C atom on the pyrazole ring. Two schematic, one-dimensional projections of the multidimensional singlet potential energy surfaces (S_0, S_1, and S_2) of DNP for each NO_2 group as a separate active site: locations and potential energies for different critical points and conical intersections are shown in Figures 7 and 4S.[39] Arrows in Figures 7 and 4S indicate different possible decomposition channels for DNP. Structures of each critical points and conical intersections, for each NO_2 group as different reaction sites, are summarized in Figures 8 and 5S:[39] arrows near the transition states and conical intersections show the imaginary frequencies. The optimized x, y, z coordinates in angstroms of all the stationary points for the 3,4-dinitrpyrazole reaction are shown in Tables IS(c) and IS(d) in the supplementary material.[39] As shown in Figures 7 and 4S, the behavior of DNP is similar to the nitropyrazole model systems at the beginning of the reaction pathway. DNP undergoes a rapid internal conversion from S_2 to S_1 through the $(S_2/S_1)_{CI}$ conical intersection following excitation without an energy barrier. Because no significant change occurs in the nuclear configuration of DNP (only a small rotation of the two NO_2 groups), the two NO_2 groups in Figures 8 and 5S have similar $(S_2/S_1)_{CI}$ structures. The adiabatic energy gap between the S_1 and S_2 surfaces near $(S_1/S_2)_{CI}$ is computed to be 13 cm^{-1}, suggesting that the S_1 and S_2 surfaces are strongly nonadiabatically coupled at this point. On the S_1 state surface, different from the model systems, the transition state energies in Figures 7 and 4S for DNP S_1 state decomposition are 6.95 eV and 6.01 eV, respectively, and both of them are higher than the excitation energy limit of 5.5 eV. Therefore, DNP does not have enough

energy to surmount the transition state $S_{1,TS2}$ threshold to produce NO on the S_1 potential energy surface. In this case, only the nonadiabatic relaxation pathway through $(S_1/S_0)_{CI}$ is open for DNP. The S_1 potential energy surface of DNP can lead to a nonadiabatically coupled conical intersection from the S_1 surface to the S_0 surface through $(S_1/S_0)_{CI}$ following the minimum energy path. The molecule isomerizes to the nitrite form on its S_0 surface and undergoes NO elimination, surmounting a small energy barrier ($\sim$0.70–0.88 eV) to the nitro-nitrite isomerization transition state. This conical intersection is energetically accessible and the molecule can rapidly come back to the ground state transferring electronic excitation energy to its vibrational degrees of freedom. The structure near $(S_1/S_0)_{CI}$ is a loose nitro-nitrite transition state geometry for which an NO_2 moiety at the related active site of DNP interacts with the rest of the molecule from a long distance ($\sim$3.0 A) for the different NO_2 groups. This NO_2 group has an out of plane NO_2 bending mode with respect to the C-NO_2 plane: near $(S_1/S_0)_{CI}$ the energy differences between S_1 and S_0 for the two NO_2 group are 15 cm^{-1} (C3) and 4 cm^{-1} (C4), respectively. No torque is applied to NO during the decomposition along this reaction coordinate, thus the NO product should have a cold rotational temperature, consistent with experimental results. In sum, DNP can only decompose on its S_0 ground state under all excitation conditions, generating cold rotational and hot vibrational temperatures for the NO initial product. Initial decomposition for either of the two NO_2 groups at C3 or C4 positions of the pyrazole ring is energetically and structurally quite similar.

The most significant difference between the energetic system DNP and model systems 4-nitropyrazole and 1-nitropyrazole, is that the model systems have two competitive decomposition pathways: model molecules can form NO product in either S_0 or S_1 state, while the energetic system can only decompose in the ground state S_0, in which more vibrational energy is stored. The difference is manifested in the experimental results, as the NO product from DNP is 1350 K vibrationally hotter than that from the model species. From our previous study on energetic/model systems, the NO product from energetic materials usually has cold rotational temperature and hot vibrational temperature while from model material the NO product is usually rotationally hot and vibrationally cold.[25–27,29–32,34–38] DNP behavior is consistent with that of previous studies of energetics, while these model systems display somewhat different behavior from that of other model systems. Nonetheless, both mono-nitropyrazoles and -nitroimidazoles display similar internal energy distributions for the initial NO product. Both nitropyrazoles and nitroimidazoles have aromatic rings that have a significant affect the reaction pathways; moreover, their first few electronic excited states are of a similar orbital excitation description involving $n\pi^*$ transition on local NO_2 groups. The rotational excitation of the NO product depends on the structure and reaction coordinate of the final transition state for the decomposing parent molecule. The vibrational excitation of NO depends on the stored vibrational energy in the particular electronic state in which the decomposition occurs (e.g., S_0 or S_1 in this instance). The general result is that for all NO_2 containing

energetic materials decomposition following electronic excitation, NO is the initial product from S_0 with a higher degree of vibrational excitation than found for comparable model species, which typically decompose from an excited electronic state.

The vibrational temperature of the initial dissociation product is important in recognizing energetic molecules because initial decomposition products with high vibrational excitation are able to propagate a chain reaction, following the initial stimulus, which leads to detonation. The model molecules do not have an efficient single pathway to release their entire chemically stored energy during the excited electronic state decomposition process. Multi-nitropyrazoles descend to the ground state through a series of conical intersections and dissociate on the ground state PES after nitro-nitrite isomerization to produce an NO initial decomposition product. This $S_n \rightarrow \ldots \rightarrow S_o$ pathway through a series of conical intersections leaves the molecule on a new part of the S_0 potential energy surface, not necessary near the FC equilibrium point.[31,32] Thereby, all the excitation energy is available to break internal bonds to generate reactive fragments and radicals for further reactions as maybe required to be classified as an energetic molecule.

VI. CONCLUSIONS

The decomposition of the energetic material DNP and two model materials 4-nitropyraozle and 1-nitropyrazole following electronic excitation has been explored via nanosecond, energy resolved spectroscopy. These materials create NO as an initial decomposition product at the nanosecond excitation energies (5.0–5.5 eV) with vibrationally hot (model system 2300 $\pm$ 300 K, DNP 3850 $\pm$ 50 K) and rotationally cold (<60 K) NO product. Based on the experimental observations and CASSCF theoretical calculations, we conclude that for the mono-nitropyrazole model systems, a competition of molecular decomposition on both the S_1 excited and S_0 ground electronic states is possible, with S_1 state decomposition more probable. For the energetic DNP, decomposition occurs on the S_0 state potential energy surface, as S_1 state decomposition is energetically unavailable. Molecules excited to the S_2 state descend to the S_1 and S_0 states through $(S_2/S_1)_{CI}$ and $(S_1/S_0)_{CI}$ conical intersections, and NO is generated following a nitro-nitrite isomerization either on the S_1 potential energy surface (model system) or S_0 surface (DNP, small percent of model systems). Conical intersections are the key point for the theoretical mechanisms, as they provide nonadiabatic radiationless internal conversion between upper and lower electronic states on the fs time scale. For all NO_2 containing energetic material studied at the present kinetic and dynamic level of detail, vibrational temperature of the NO product from the energetic materials is at least 1000 K higher than that for their related model systems. Each energetic system decomposes on a lower electronic state surface than its models do: during this process, more stored plus excitation energy can be released to propagate a chain reaction following the initial stimulus that leads to detonation.

ACKNOWLEDGMENTS

[1] B. M. Rice, S. Sahu, and F. J. Owens, J. Mol. Struct.: THEOCHEM **583**, 69 (2002).

[2] B. Tan, X. Long, R. Peng, H. Li, B. Jin, S. Chu, and H. Dong, J. Hazard. Mater. **183**, 908 (2010).

[3] M. R. Manaa, L. E. Fried, C. F. Melius, M. Elstner, and Th. Frauenheim, J. Phys. Chem. A **106**, 9024 (2002).

[4] A. B. Kunz, M. M. Kuklja, T. R. Botcher, and T. P. Russell, Thermochim. Acta **384**, 279 (2002).

[5] M. M. Kuklja, J. Appl. Phys. **89**, 4156 (2001).

[6] E. J. Reed, J. D. Joannopoulos, and L. E. Fried, Phys. Rev. B **62**, 16500 (2000).

[7] K. E. Gutowski, R. D. Rogers, and D. A. Dixon, J. Phys. Chem. A **110**, 11890 (2006).

[8] K. E. Gutowski, R. D. Rogers, and D. A. Dixon, J. Phys. Chem. B **111**, 4788 (2007).

[9] S. Du, Y. Wang, L. Chen, W. Shi, F. Ren, Y. Li, J. Wang, and D. Cao, J. Mol. Model. **18**, 2105 (2012).

[10] S. Blanco, J. C. Lopez, J. L. Alonso, O. Mo, M. Yanez, N. Jagerovic, and J. Elguero, J. Mol. Struct. **344**, 241 (1995).

[11] I. L. Dalinger, D. V. Khakimov, T. K. Shkineva, I. A. Vatsadze, G. P. Popova, T. S. Pivina, and S. A. Shevelev, Chem. Heterocycl. Compd. **48**, 1646 (2013).

[12] R. K. Toghiani, H. Toghiani, S. W. Maloney, and V. M. Boddu, Fluid Phase Equilib. **264**, 86 (2008).

[13] E. N. Rao, P. Ravi, Surya P. Tewari, and S. V. Rao, J. Mol. Struct. **1043**, 121 (2013).

[14] D. Dumanovic, J. Ciric, A. Muk, and V. Nikolic, Talanta **22**, 819 (1975).

[15] P. Ravi, A. A. Vargeese, and S. P. Tewari, Thermochim. Acta **550**, 83 (2012).

[16] F. Yehya and A. K. Chaudhary, Appl. Phys. B **110**, 15 (2013).

[17] J. M. Abboud, R. Notario, M. Yanez, O. Mo, R. Flammang, N. Jagerovic, I. Alkorta, and J. Elguero, J. Phys. Org. Chem. **12**, 787 (1999).

[18] M. R. Manaa and L. E. Fried, J. Phys. Chem. A **103**, 9349 (1999).

[19] B. Tan, R. Peng, X. Long, H. Li, B. Jin, and S. Chu, J. Mol. Model. **18**, 583 (2012).

[20] B. Tan, X. Long, J. Li, F. Nie, and J. Huang, J. Mol. Model. **18**, 5127 (2012).

[21] A. B. Kunz and D. R. Beck, Phys. Rev. B **36**, 7580 (1987).

[22] C. M. Tarver, AIP. Conf. Proc. **1426**, 227 (2012).

[23] S. H. Lee, K. C. Tang, I. C. Chen, M. Schmitt, J. P. Shaffer, T. Schultz, J. G. Underwood, M. Z. Zgierski, and A. Stolow, J. Phys Chem. A **106**, 8979 (2002).

[24] A. Bhattacharya, Y. Q. Guo, and E. R. Bernstein, Acc. Chem. Res. **43**, 1476 (2010).

[25] Y. Q. Guo, A. Bhattacharya, and E. R. Bernstein, J. Chem. Phys. **122**, 244310 (2005).

[26] Y. Q. Guo, M. Greemfield, A. Bhattacharya, and E. R. Bernstein, J. Chem. Phys. **127**, 154301 (2007).

[27] A. Bhattacharya, Y. Q. Guo, and E. R. Bernstein, J. Chem. Phys. **131**, 194304 (2009).

[28] C. J. S. M. Simpson, P. T. Griffiths, H. L. Wallaart, and M. Towrie, Chem. Phys. Lett. **263**, 19 (1996).

[29] A. Bhattacharya, Y. Q. Guo, and E. R. Bernstein, J. Phys. Chem. A **113**, 811 (2009).

[30] Z. Yu and E. R. Bernstein, J. Chem. Phys. **135**, 154305 (2011).

[31] Z. Yu and E. R. Bernstein, J. Chem. Phys. **137**, 114303 (2012).

[32] Z. Yu and E. R. Bernstein, J. Phys. Chem. **117**, 1756 (2013).

[33] A. I. Vokin, T. N. Komarova, L. I. Larina, and V. A. Lopyrev, Russ. Chem. Bull. **46**, 297 (1997).

[34] L. Larina and L. Lopyrev, *Nitroazoles: Synthesis, Structure and Applications* (Springer, New York, 2009).

[35] Y. Q. Guo, A. Bhattacharya, and E. R. Bernstein, J. Chem. Phys. **134**, 024318 (2011).

[36] Y. Q. Guo, A. Bhattacharya, and E. R. Bernstein, J. Chem. Phys. **128**, 034303 (2008).

[37] A. Bhattacharya and E. R. Bernstein, J. Phys. Chem. A **115**, 4135 (2011).

[38] Y. Q. Guo, A. Bhattacharya, and E. R. Bernstein, J. Phys. Chem. A **115**, 9349 (2011).

[39] See supplementary material at http://dx.doi.org/10.1063/1.4861670 for the optimized x, y, z coordinates of the stationary points in all three reactions, experimental result for 1-nitropyrazole, theoretical reaction mechanisms and structures of stationary points for 1-nitropyrazole and 3,4-nitropyrazole(C3) reactions.